Online Appendix: Description of Modeling Framework

A.1 Age-structured model

The age-structured model is identical to the single-strain model, except that the infected cells committed to the asexual cycle are split into young and mature classes (I_y and I_m, respectively), both with fixed development times (α_y and α_m, respectively). Saturating immunity targets only the mature infected red blood cells (I_m), so Eq. 4 becomes

$$\begin{aligned}
\frac{dI_y(t)}{dt} &= (1-c)p(t)R(t)M(t) - \mu I_y(t) \\
&\quad -(1-c)p(t-\alpha_y)R(t-\alpha_y)M(t-\alpha_y)\exp(-\mu\alpha_y) \\
\frac{dI_m(t)}{dt} &= (1-c)p(t-\alpha_y)R(t-\alpha_y)M(t-\alpha_y)exp(-\mu\alpha_y) - \mu I_m(t) - \frac{a}{b+I_m(t)}I_m(t) \\
&\quad -(1-c)p(t-\alpha)R(t-\alpha)M(t-\alpha)S_m
\end{aligned} \tag{A1}$$

where the survivorship is the mortality rates integrated over the respective developmental periods

$$S_m = \exp\left(-\int_{t-\alpha_y-\alpha_m}^{t-\alpha_m} \mu d\omega - \int_{t-\alpha_m}^{t} \mu + \frac{a}{b+I_m(\omega)} d\omega\right) \tag{A2}$$

A.2 Two strain model

The coinfection model tracks infected red blood cells (sexual and asexual), merozoites, and gametocytes for two strains in complete analogy to our single-strain model.

$$\begin{aligned}\frac{dR(t)}{dt} &= \lambda\left(1-\frac{R(t)}{K_{start}}\right) \\ &\quad -\mu R(t) - p(t)R(t)M_1(t) - p(t)R(t)M_2(t)\end{aligned} \tag{A3}$$

where I_A indicates asexual infected red blood cells of both strains ($I_1 + I_2$).

$$\begin{aligned}\frac{dI_1(t)}{dt} &= (1-c)p(t)R(t)M_1(t) - \mu I_1(t) - \frac{a}{b+I_A(t)}I_1(t) \\ &\quad -(1-c)p(t-\alpha)R(t-\alpha)M_1(t-\alpha)\exp\left(-\left[\int_{t-\alpha}^{t}\mu + \frac{a}{b+I_A(\omega)}d\omega\right]\right)\end{aligned} \tag{A4}$$

$$\begin{aligned}\frac{dI_2(t)}{dt} &= (1-c)p(t)R(t)M_2(t) - \mu I_2(t) - \frac{a}{b+I_A(t)}I_2(t) \\ &\quad -(1-c)p(t-\alpha)R(t-\alpha)M_2(t-\alpha)\exp\left(-\left[\int_{t-\alpha}^{t}\mu + \frac{a}{b+I_A(\omega)}d\omega\right]\right)\end{aligned} \tag{A5}$$

$$\begin{aligned}\frac{dM_1(t)}{dt} &= \beta(1-c)p(t-\alpha)R(t-\alpha)M_1(t-\alpha)\exp\left(-\left[\int_{t-\alpha}^{t}\mu + \frac{a}{b+I_A(\omega)}d\omega\right]\right) \\ &\quad -p(t)R(t)M_1(t) - \mu_Z M_1(t)\end{aligned} \tag{A6}$$

$$\begin{aligned}\frac{dM_2(t)}{dt} &= \beta(1-c)p(t-\alpha)R(t-\alpha)M_2(t-\alpha)\exp\left(-\left[\int_{t-\alpha}^{t}\mu + \frac{a}{b+I_A(\omega)}d\omega\right]\right) \\ &\quad -p(t)R(t)M_2(t) - \mu_Z M_2(t)\end{aligned} \tag{A7}$$

$$\frac{dI_{G1}(t)}{dt} = cp(t)R(t)M_1(t) - \mu I_{G1}(t) - cp(t-\alpha_G)R(t-\alpha_G)M_1(t-\alpha_G)\exp(-\mu\alpha_G) \tag{A8}$$

$$\frac{dI_{G2}(t)}{dt} = cp(t)R(t)M_2(t) - \mu I_{G2}(t) - cp(t-\alpha_G)R(t-\alpha_G)M_2(t-\alpha_G)\exp(-\mu\alpha_G) \tag{A9}$$

$$\frac{dG_1(t)}{dt} = cp(t-\alpha_G)R(t-\alpha_G)M_1(t-\alpha_G)\exp(-\mu\alpha_G) - \mu_G G_1(t) \tag{A10}$$

$$\frac{dG_2(t)}{dt} = cp(t-\alpha_G)R(t-\alpha_G)M_2(t-\alpha_G)\exp(-\mu\alpha_G) - \mu_G G_2(t) \tag{A11}$$

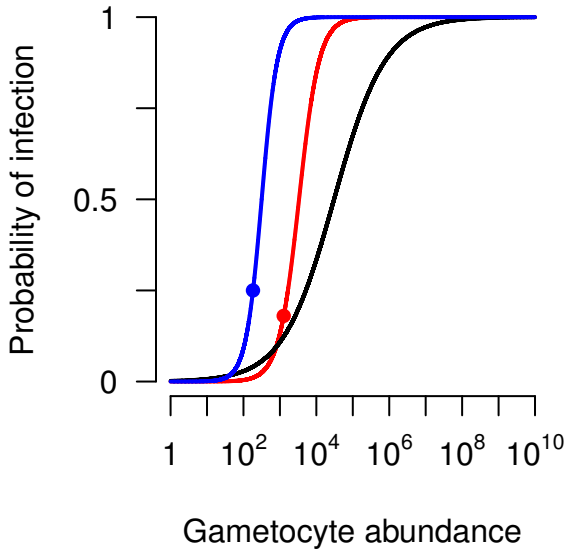

Figure A1: Extremes in transmission biology: the probability of transmission is shown as a function of gametocyte abundance for drug-sensitive *P. chabaudi* (red, Eqn. 13), drug-resistant *P. chabaudi* (black, *probability of transmission* $= \exp(-6.37 + 1.42\log_{10} G(t))/(1+\exp(-6.37 + 1.42\log_{10} G(t)))$, and *P. falciparum* (blue, *probability of transmission* $= 1\times 10^{-5} G(t)^2/(1+1\times 10^{-5} G(t)^2)$). Equations and parameter values from curves fit to data by Huijben et al. 2010 and Bell et al. 2012. Red and blue dots represent the inflection points for *P. chabaudi* (drug-sensitive) and *P. falciparum*, respectively, i.e., where the curve switches from accelerating to saturating. The drug-sensitive *P. chabaudi* curve was used for all simulations in the main text. Its inflection point falls below a 50% probability of infection—even though it is derived from a logistic regression—because it is a function of the $\log_{10}$ abundance of gametocytes and the chain rule applies. Note the absence of an inflection point on the drug-resistant *P. chabaudi* curve. Despite its appearance on a log scale, the black curve is saturating over the entire range.

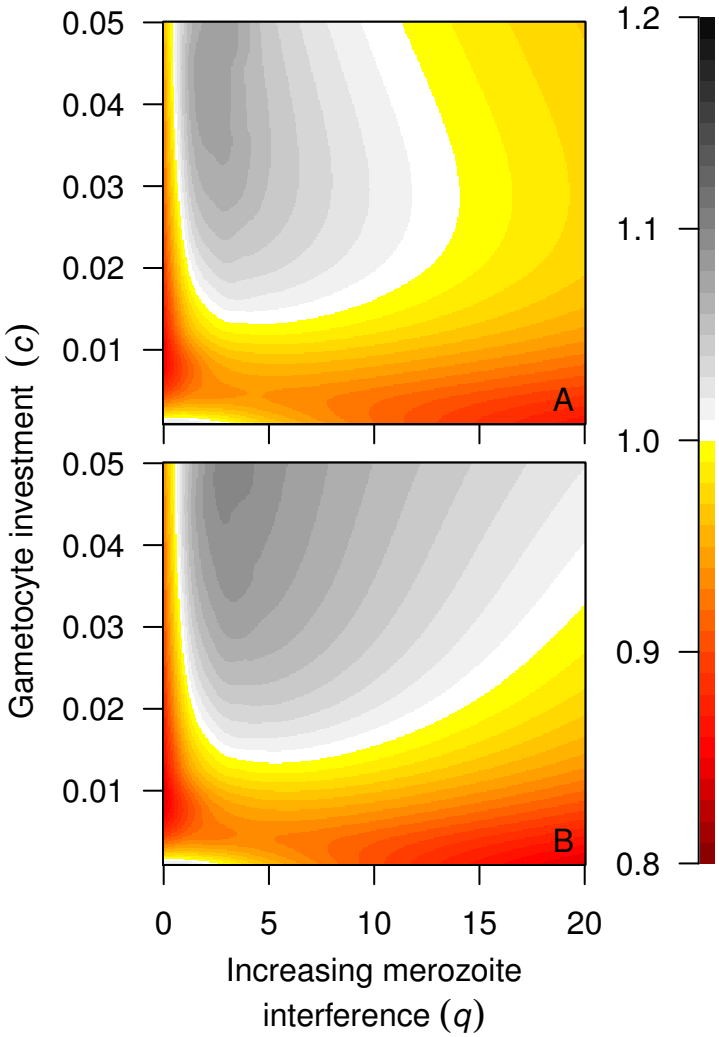

Figure A2: Smoothed relative fitness of synchronous:asynchronous infections either for no immunity (A, $a = 0$) or for immunity targeting infected red blood cells in the last hour before bursting (B, $a = 1800$, $b = 100$). Younger infected red blood cells are not subject to immune clearance. Panel A is identical to fig. 5A, and is placed here for comparison.

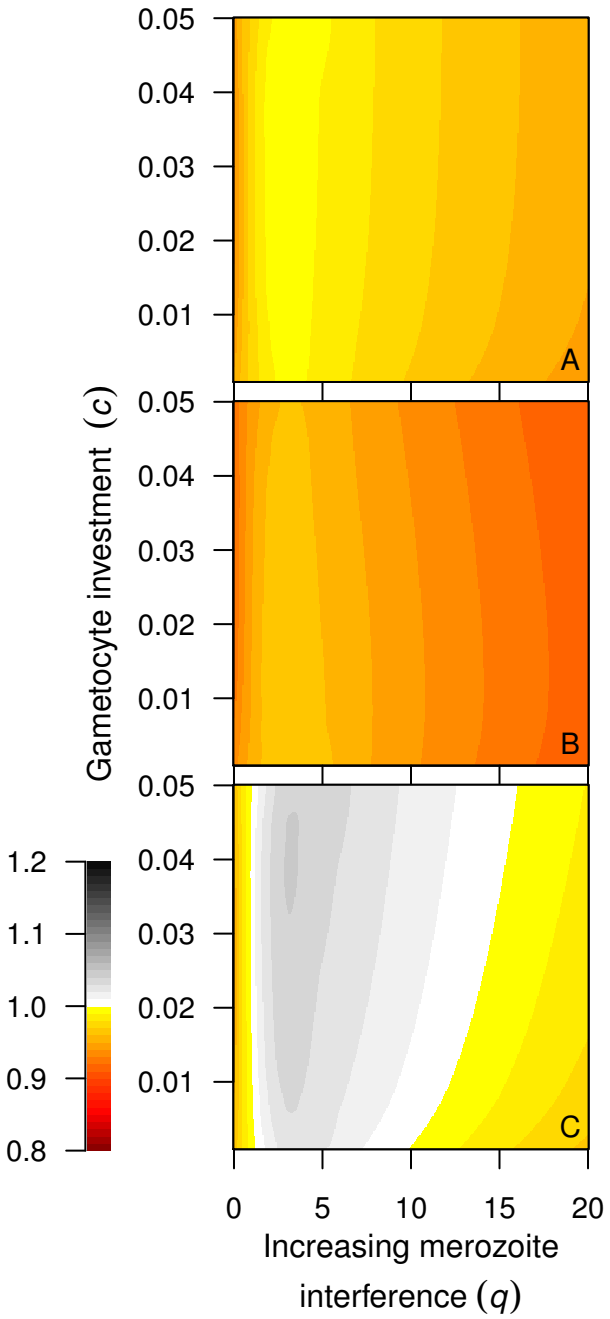

Figure A3: Smoothed relative fitness in single infections (ratio of cumulative transmission for synchronous:asynchronous strain) calculated using the drug-resistant *P. chabaudi* transmission function (black curve in fig. A1). Otherwise, dynamics are identical to fig. 5. Since the transmission function is entirely saturating, the relative fitness does not vary much with changes in gametocyte investment.

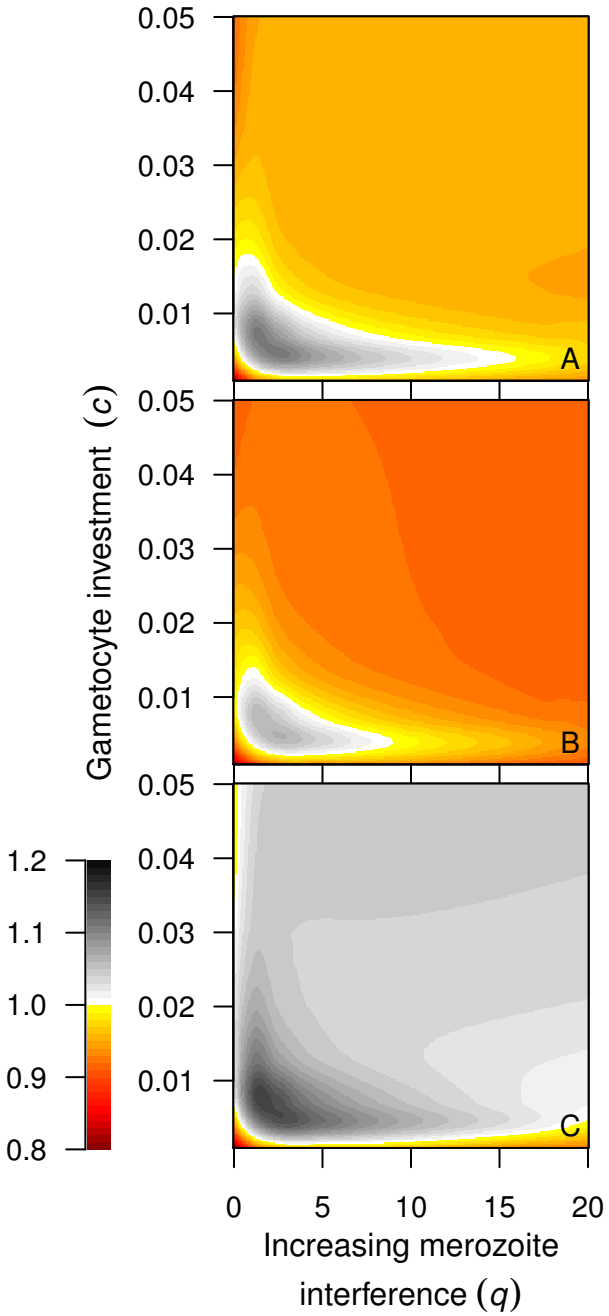

Figure A4: Smoothed relative fitness in single infections (ratio of cumulative transmission for synchronous:asynchronous strain) calculated using the *P. falciparum* transmission function (blue curve in fig. A1). Save for the calculation of relative fitness, dynamics are identical to fig. 5. Since the transmission function saturates earlier, a smaller region of the parameter space is favorable to synchronous parasites in the absence of immunity.

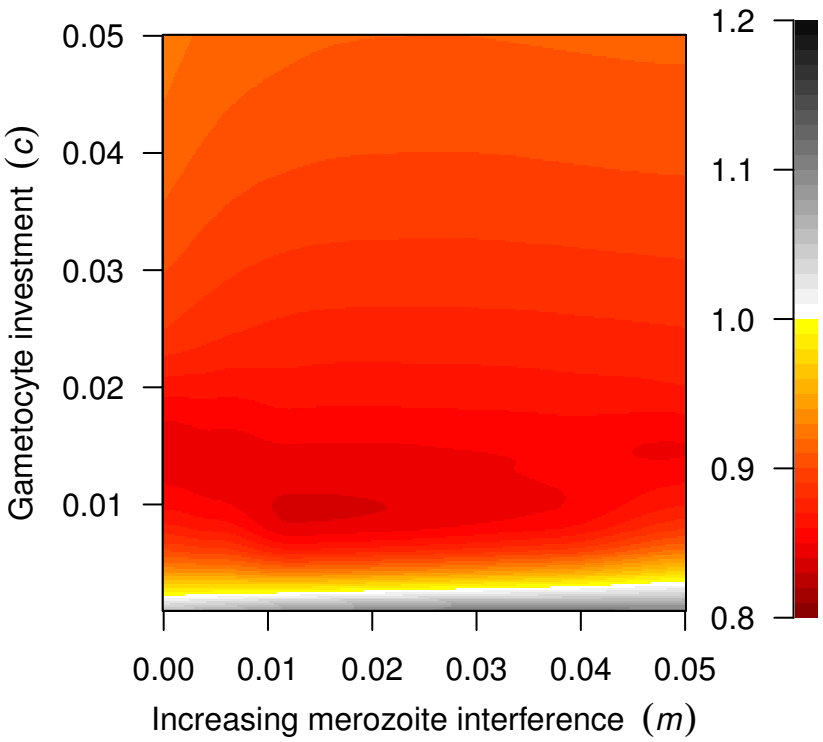

Figure A5: Smoothed relative fitness in single infections (ratio of mean transmission for synchronous:asynchronous strain) using an alternate form of merozoite interference ($z(t)$, Eqn. 3). Parameters otherwise identical to fig. 5 (i.e., relative fitness calculated with Eqn. 13).

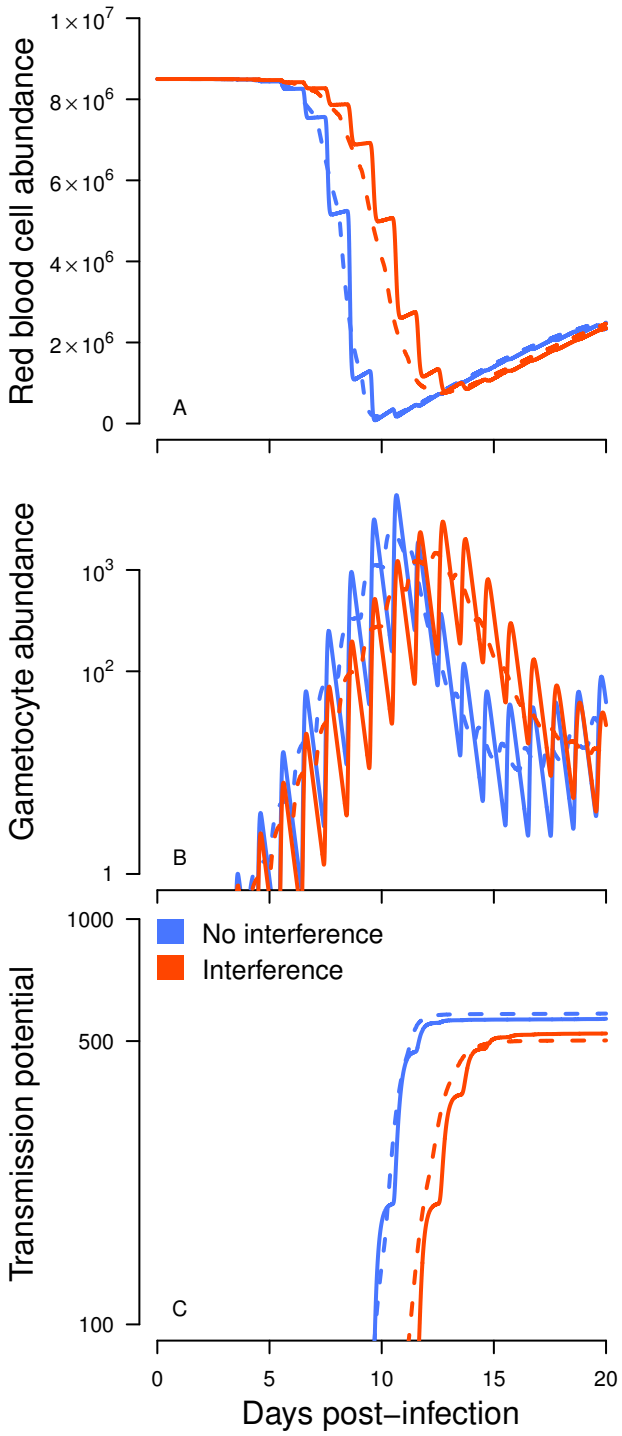

Figure A6: Red blood cell abundance (A), gametocyte abundance (B), and transmission potential (C, cumulative probability of transmission) simulated for parasitoid-like merozoite interference (Eqn. 3), with $m = 0.05$ for orange curves. Synchronous dynamics are again shown in solid lines while asynchronous infections are denoted with dashed lines. Gametocyte investment was set low ($c = 0.002$), and immunity was absent ($a = 0$). Transmission potential was calculated using Eqn. 13. Synchronous strains can benefit from merozoite competition (C, orange lines), while the asynchronous infection would have transmitted better in the absence of competition (C, blue lines).

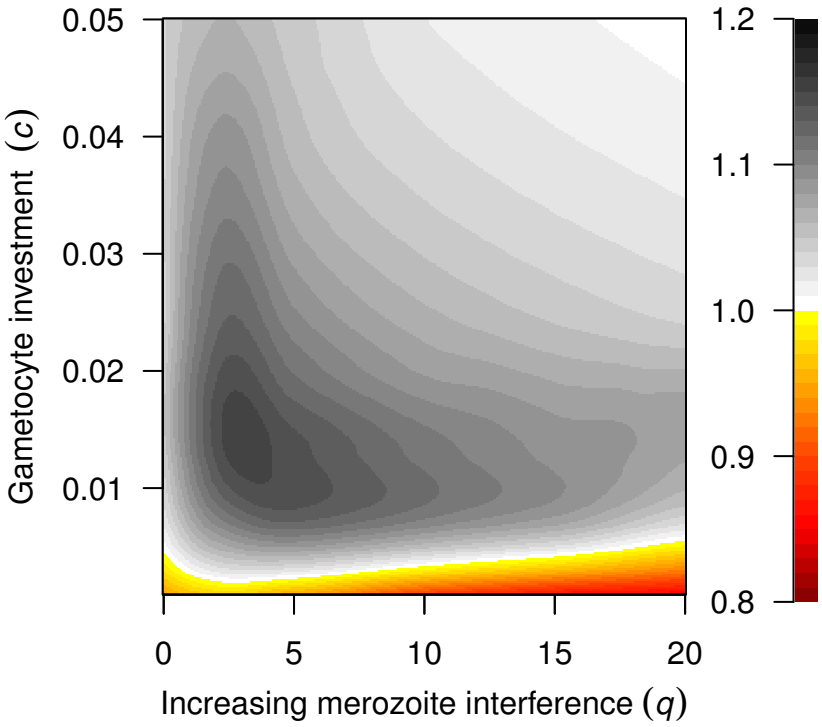

Figure A7: Smoothed relative fitness of synchronous:asynchronous infections as shown in fig. 5A, except that gametocytes have a mean infectious lifespan of approximately 20 hours (based on data in Reece et al. 2003) instead of six hours (from data in Gautret et al. 1996).

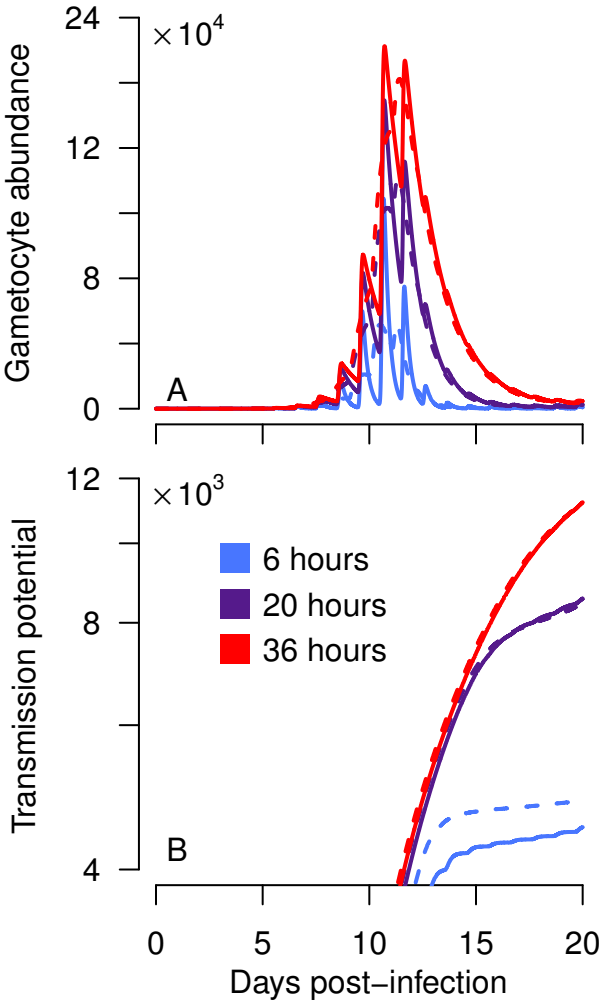

Figure A8: Gametocyte abundance (A) and the transmission potential (i.e., the cumulative probability of transmission) (B) as gametocyte longevity increases. Asynchronous dynamics are given by dashed lines, and synchronized infections are shown with solid lines. Merozoite interference is absent ($q = 0$), and there is relatively high investment in gametocytes ($c = 0.05$). Increasing gametocyte longevity to 20 hours give synchronous strains an advantage, but increasing longevity still further—such that gametocytes outlive asexual forms—sharply reduces transmission differences between synchronous and asynchronous parasites.